ISTANBUL TECHNICAL UNIVERSITY ★ INSTITUTE OF SCIENCE AND TECHNOLOGY

GLOBAL PHASE DIAGRAMS OF BEG SPIN-GLASS AND SPINLESS FERMION SYSTEMS

M.Sc. Thesis by

Veli Ongun ÖZÇELİK

Department : Physics Engineering

Programme : Physics Engineering

JUNE 2008

ISTANBUL TECHNICAL UNIVERSITY ★ INSTITUTE OF SCIENCE AND TECHNOLOGY

GLOBAL PHASE DIAGRAMS OF BEG SPIN-GLASS AND SPINLESS FERMION SYSTEMS

M.Sc. Thesis by

Veli Ongun ÖZÇELİK
509051117

Date of submission : 5 May 2008
Date of defence examination: 11 June 2008

Supervisors (Chairmen):
Prof. Dr. A. Nihat Berker (KU)
Prof. Dr. Ahmet Giz (ITU)

Members of the Examining Committee:
Assoc. Prof. Dr. Haluk Özbek (ITU)
Assoc. Prof. Dr. Ferid Salehli (ITU)
Assoc. Prof. Dr. Muhittin Mungan (BU)

JUNE 2008

İSTANBUL TEKNİK ÜNİVERSİTESİ ★ FEN BİLİMLERİ ENSTİTÜSÜ

BEG SPIN CAMININ GLOBAL FAZ DİYAGRAMLARI VE SPİNSİZ FERMİYON SİSTEMLERİ

Yüksek Lisans Tezi

Veli Ongun ÖZÇELİK
509051117

Tezin Enstitüye Verildiği Tarih : 5 Mayıs 2008
Tezin Savunulduğu Tarih : 11 Haziran 2008

Tez Danışmanları :	**Prof. Dr. A. Nihat Berker (KÜ)**
	Prof. Dr. Ahmet Giz (İTÜ)
Diğer Jüri Üyeleri :	**Doç. Dr. Haluk Özbek (İTÜ)**
	Doç. Dr. Ferid Salehli (İTÜ)
	Doç. Dr. Muhittin Mungan (BÜ)

HAZİRAN 2008

"Anyone who has common sense will remember that the bewilderment of the eyes are of two kinds and arise from two causes, either from coming out of the light or from going into the light, and, judging that the soul may be affected in the same way, will not give way to foolish laughter when he sees anyone whose vision is perplexed and weak; he will first ask whether that soul of man has come out of the brighter life and is unable to see because unaccustomed to the dark, or having turned from darkness to the day is dazzled by excess of light."

Plato, *The Republic*

ACKNOWLEDGEMENT

I would like to express my thanks and gratitude to my advisor Prof. Nihat Berker for his relentless efforts, advice and encouragement during my studies in ITU. I appreciate the useful help of Michael Hinczewski for guiding me in the second part of the thesis. I would also like to thank the professors at ITU and especially Prof. Ahmet Giz for being the co-advisor of the project.

June 2008 Veli Ongun ÖZÇELİK

TABLE OF CONTENTS

ABBREVATIONS

RG	:	Renormalization-group
BEG	:	Blume-Emery-Griffiths
SG	:	Spin-glass

LIST OF TABLES

LIST OF FIGURES

LIST OF SYMBOLS

$\mathbf{d}$	:	Lattice dimension
$\mathbf{b}$	:	Length rescaling factor
$\mathbf{i,j,k}$	:	Sites on lattice
$\mathscr{H}$	:	Hamiltonian
$\mathbf{k}$	:	Boltzmann constant
T	:	Temperature
T_c	:	Critical temperature
$\mathbf{M}$	:	Magnetization
$\mathbf{H}$	:	External field
F	:	Free energy
$\mathbf{Z}$	:	Partition function
$\mathbf{E}$	:	Total energy
m	:	Order parameter
$\mathbf{N}$	:	Number of particles, bonds
λ	:	Critical exponent
C_H	:	Specific heat
χ	:	Susceptibility
ξ	:	Correlation length
J	:	Linear exchange coefficient
K	:	Quadratic exchange coefficient
Δ	:	Crystal-field interaction
s	:	Classical Ising spin
p	:	Antiferromagnetic bond concentration
t	:	Electron hopping strength
U	:	On-site interaction strength
μ	:	Chemical potential
$c_i^\dagger, c_i$	:	Creation and destruction operators
u, v, w	:	Single-site quantum states
ϕ, Ψ	:	Two- and three-site eigenstates
$\hat{T}$	:	Recursion matrix

GLOBAL PHASE DIAGRAMS OF BEG SPIN-GLASS AND SPINLESS FERMION SYSTEMS

SUMMARY

Throughout this thesis, attention was given to phase transitions taking place in classical and quantum systems with specific renormalization-group transformation applications to the Blume-Emery-Griffiths (BEG) model and the Hubbard model. The Blume-Emery-Griffiths model is a useful system for the study of the various meetings of first- and second-order phase boundaries between ordered and disordered phases, in a plethora of phase diagram topologies. This model has already been used to describe ^{3}He-^{4}He mixtures, solid-liquid-crystal-gas systems, multicomponent fluid and liquid-crystal mixtures, microemulsions, semiconductor alloys, and electronic conduction systems. In this study with the inclusion of frozen disorder (quenched randomness) to the BEG system and by calculating the global phase diagram of the Blume-Emery-Griffiths spin-glass model, the phase boundaries in that system were investigated and an inverted tricritical point behavior was observed. Also, a strong-coupling second-order phase transition was observed between the paramagnetic and ferromagnetic phases. In the topologies of the calculated phase diagrams, spin-glass and paramagnetic reentrances were seen. The phase diagrams were determined by the basins of attraction of the renormalization-group sinks, namely the completely stable fixed points and fixed distributions. In the second part of the thesis, the phase diagrams and expectation values of the interaction terms were obtained for the hard-core fermionic Hubbard model which is a simple but realistic model for describing electronic systems. In the investigated model it was found that the system had four different phases, all of which were separated by second-order phase transitions. The phases found were a dilute phase, a dense phase, and two intermediate phases characterized by enhanced fermion hopping.

BEG SPIN CAMININ GLOBAL FAZ DİYAGRAMLARI VE SPİNSİZ FERMİYON SİSTEMLERİ

ÖZET

Bu tez sürecinde klasik ve kuantum sistemlerde meydana gelen faz geçişleri üzerinde durularak Blume-Emery-Griffiths ve Hubbard modelleri üzerinde uygulamalar yapılmıştır. Blume-Emery-Griffiths modeli, düzenli ve düzensiz fazlar arasındaki birinci ve ikinci derece faz sınırlarının buluşmalarını inclemek için faydalı bir karmaşık sistemdir. Bu model daha önce ^{3}He-^{4}He karışımlarını, katı-sıvı-kristal-gaz sistemlerini, çok bileşenli akışkan ve sıvı-kristal sistemlerini, mikro emülsüyonları, yarı iletken alaşımları, ve elektronik iletim sistemlerini açıklamak için kullanılmıştır. Bu çalışmada, sisteme donmuş düzensizlikler eklenerek Blume-Emery-Griffiths spin camı modelinin global faz diyagramları hesaplanmış, bu faz diyagramları üzerindeki faz sınırları incelenmiş; birinci ve ikinci dereceden faz geçişlerini ayıran trikritik noktanın sıcaklığa olan ters bağlılığı gözlemlenmiştir. Ayrıca, paramagnetik ve ferromagnetik fazlar arasında kuvvetli etkileşimli ikinci dereceden bir faz geçişi gözlemlenmiştir. Hesaplanan faz diyagramlarının topolojisinde spin camı ve paramagnetik geri dönüşlerine raslanmıştır. Faz diyagramları ve geçişleri hesaplanırken, Hamiltonyende yer alan etkileşim katsayılarının renormalizasyon grubu dönüşümü altında gittikleri sabit noktalardan veya sabit dağılımlardan faydalanılmıştır. Tezin ikinci kısmında, elektronik sistemleri açıklamak için basit fakat gerçekçi bir model olan Hubbard modeli üzerinde durularak, fermiyon sistemlerinin faz diyagramları ve etkileşim sabitlerinin yoğunluklar hesaplanmıştır. Yoğun, seyrek ve iki ara fazdan oluşan bu sistemde bütün faz geçişlerinin ikinci dereceden olduğu yapılan özdeğer üsteli hesaplamaları sonucunda görülmüştür.

1. INTRODUCTION

1.1 Phase Transitions and Critical Phenomena

Everyone has experienced the occurrence of a phase transition while watching a cold rainy day from their window and drawing figures on the foggy glass, hoping to add some enjoyment to the day alone at home by changing the phase of the condensed water particles. Having greatly enjoyed this action, in order to have a better understanding of the laws of nature, investigating the thermodynamic events taking place during this phenomenon might be a good next step to take. In nature, thermodynamic systems can be in different phases depending on their conditions. Passing from one phase to another is named a phase transition and during this transition one or more of the properties of the system can vary spontaneously. It is possible to find various physical systems which experience a phase transition when one of the intensive physical quantities characterizing the system is changed. Well-known examples of phase transitions are those between solid, liquid, and gaseous phases, the appearance of superconductivity in some metals when they are cooled under a certain temperature, or the transition of magnetic materials from the paramagnetic phase to the ferromagnetic phase at the Curie temperature. In general, it can be said that in order for a phase transition to occur, there should be a singularity in the free energy and its derivatives for some choice of the thermodynamic variables. Such non-analytical situations generally appear as a result of the interactions in many-body systems.

The most striking result of the interactions between particles is the appearance of new phases. Formally, all of the macroscopic properties of a statistical system can be derived from the partition function or the free energy. Since phase transitions typically involve sharp changes, they correspond to singularities of the free energy. Since a system formed by a finite number of particles is always going to be

analytical, a phase transition can only occur in the thermodynamic limit as a result of interactions between infinitely many particles.

A classification of phase transitions can be made based on the existence of a latent heat in the system and the level at which the singularity explained above appears. In first-order phase transitions, there exists a latent heat and the system absorbs (or emits) a fixed amount of heat from its environment. Since the energy exchange between the system and the environment will not be sudden, there is a probability of finding two phases together. In these types of phase transitions the first derivative of the free energy is discontinuous. In contrast, a second-order transition does not have a latent heat and the singularity is found in the second derivative of the free energy. Solid/liquid/gaseous systems (away from the critical point) and the paramagnetic-ferromagnetic transition of magnetic materials in zero field are examples of first-order and second-order phase transitions respectively. In Figure(1.1), the phase diagram of an Ising ferromagnet is shown.

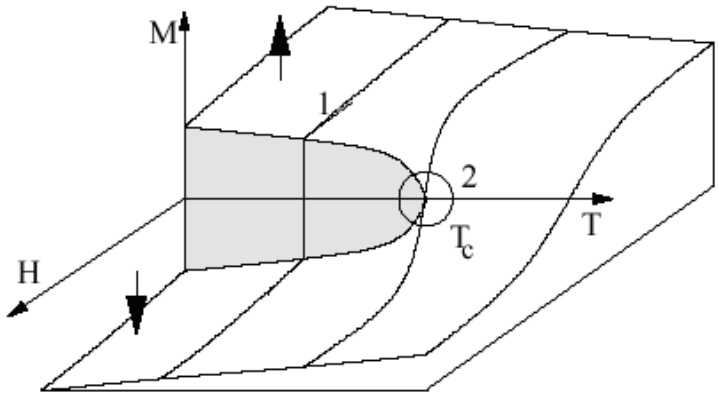

Figure 1.1: A phase diagram of an Ising magnet is shown in terms of magnetization (M), external field (H), and temperature (T). If route number 1 is followed by changing the magnetic field at a constant temperature under the critical temperature (T_c), there will be a change from a positive magnetization phase (spin up) to a negative magnetization phase (spin down). This situation is an example of a first-order phase transition. If the temperature is changed at zero magnetic field, there will be a second-order phase transition in the system at the critical temperature. In this case, the magnetization rapidly increases starting from zero when T is decreased below T_c. At the second-order phase transition point, the system suddenly chooses to be in one of the spin up or spin down phases.

By using the principles of statistical mechanics it is possible to describe physical systems in terms of intrinsic and extrinsic thermodynamical variables. Thus, the connection between statistics and thermodynamics is established by the statistical definition of the free energy

$$F(T,\mathscr{H}) = -kT\ln Z(T,\mathscr{H}), \tag{1.1}$$

where k is Boltzmann's constant, T is the temperature, $\mathscr{H}$ is the Hamiltonian of the system and Z is the partition function calculated from

$$Z(T,\mathscr{H}) = \sum_r e^{-\beta E_r}, \tag{1.2}$$

with $\beta = 1/(kT)$ and E_r representing the total energy of the system for some state r [1]. For a classical system, once the properties of all of the particles in the system are defined, the free energy can be expressed as,

$$F(T,\mathscr{H}) = -\frac{\sum_r e^{-\beta E_r}}{\beta}, \tag{1.3}$$

In the case of a quantum system, the partition function is a trace of the exponential of the Hamiltonian matrix.

The *order parameter* of a system, m, is a value that becomes non-zero below the *critical temperature*. The difference in densities between a fluid and gas phase and the magnetization in a magnetic system are examples of order parameters. A phase boundary between two phases can have both first-order and second-order phase transitions depending on the values of the interaction constants defining the system. The point separating the two different kinds of phase transitions is referred to as a *tricritical point*.

The critical properties of the system can be characterized quantitatively by examining the form of the divergences and singularities present in the derivatives of the free energy, namely the thermodynamic functions, near the critical points [2]. Allowing t to be a measure of the deviation from criticality in a function $G(t)$, for example the difference between the temperature and the critical temperature T_c,

$$t = \frac{T - T_c}{T_c}, \tag{1.4}$$

the critical exponent associated with that function is

$$\lambda = \lim_{t \to 0} \frac{\ln|G(t)|}{\ln|t|}, \tag{1.5}$$

expressing the fact that G(t) scales like

$$F(t) \sim |t|^{\lambda} \tag{1.6}$$

near T_c. A striking property of these critical exponents is that although other values characterizing phase transitions may vary widely between different systems, the critical exponents are generally dependent only on a few parameters, and whole classes of systems share the same exponent. It is this property of the critical exponents that leads to the idea of *universality*.

Table 1.1: Some critical exponents used in magnetic systems.

Zero-field specific heat	$C_H \sim \|t\|^{-\alpha}$
Zero-field magnetization	$M \sim (-t)^{\beta}$
Zero-field isothermal susceptibility	$\chi_T \sim \|t\|^{-\gamma}$
Critical isotherm	$H \sim \|M\|^{\delta}$
Correlation length	$\xi \sim \|t\|^{-\nu}$
Pair correlation function at T_c	$G(\vec{r}) \sim 1/r^{d+\eta-2}$

1.2 The Renormalization-Group Procedure

Various methods have been developed in order to understand and identify different types of phase transitions. Mean-field theories, transfer matrix formulations, high-temperature and low-temperature series expansion methods, and Monte Carlo simulations are useful tools for exploring the mysteries of critical phenomena. In this study, the renormalization-group procedure was used to derive and characterize the phase diagrams of certain classical and quantum systems.

In the most general sense, a renormalization-group transformation consists of changing the scale of a given system in order to create a mathematical relation between the physical quantities of the system at the new and old scales and then to acquire information about the system using this derived relation. The rescaling, which is the core idea of any renormalization-group transformation, can

be made by replacing a group of elements by one element which is representative of that particular group. For instance, a 3x3 block of spins containing 6 spin-up sites and 3 spin-down sites can be replaced by a single site with an up spin. By iterating this rescaling procedure, it is possible to observe how the original system behaves depending on its starting point. This rescaling keeps going until a known characteristic point is reached such that the system continues to map onto itself in successive iterations. The special characteristic points at which the renormalization-group flows stay unchanged are called *fixed points*.

In Figure(1.2), the behavior of a two-dimensional Ising model under a renormalization-group transformation is seen. At each step, nine neighboring spins were replaced by a new single spin which takes the same value as the majority of the spins in the original cluster. When this procedure was initiated far away from the critical point, the scale change shows its effect immediately and the correlation length decreases under repeated iterations. This occurs at all points, except at the critical point, where the correlation length stays the same under iteration. Therefore, by looking at the behavior of a system under a renormalization-group transformation, the critical points can be identified and the thermodynamic behavior around these points can be explained.

In general, the system may flow to a line or plane of fixed points rather than a single unique point. The type of a fixed point is related to the form of the corresponding critical exponents. For a positive critical exponent, the renormalization-group iteration will drive the system away from the fixed point. This corresponds to a relevant field. If the exponent is negative, the renormalization-group will move the system closer to the fixed point and this corresponds to an irrelevant field. Therefore, the stability of any fixed point depends on the number of relevant and irrelevant fields associated with it. A completely stable fixed point is going to have only irrelevant fields whereas an unstable fixed point is going to contain at least one relevant field.

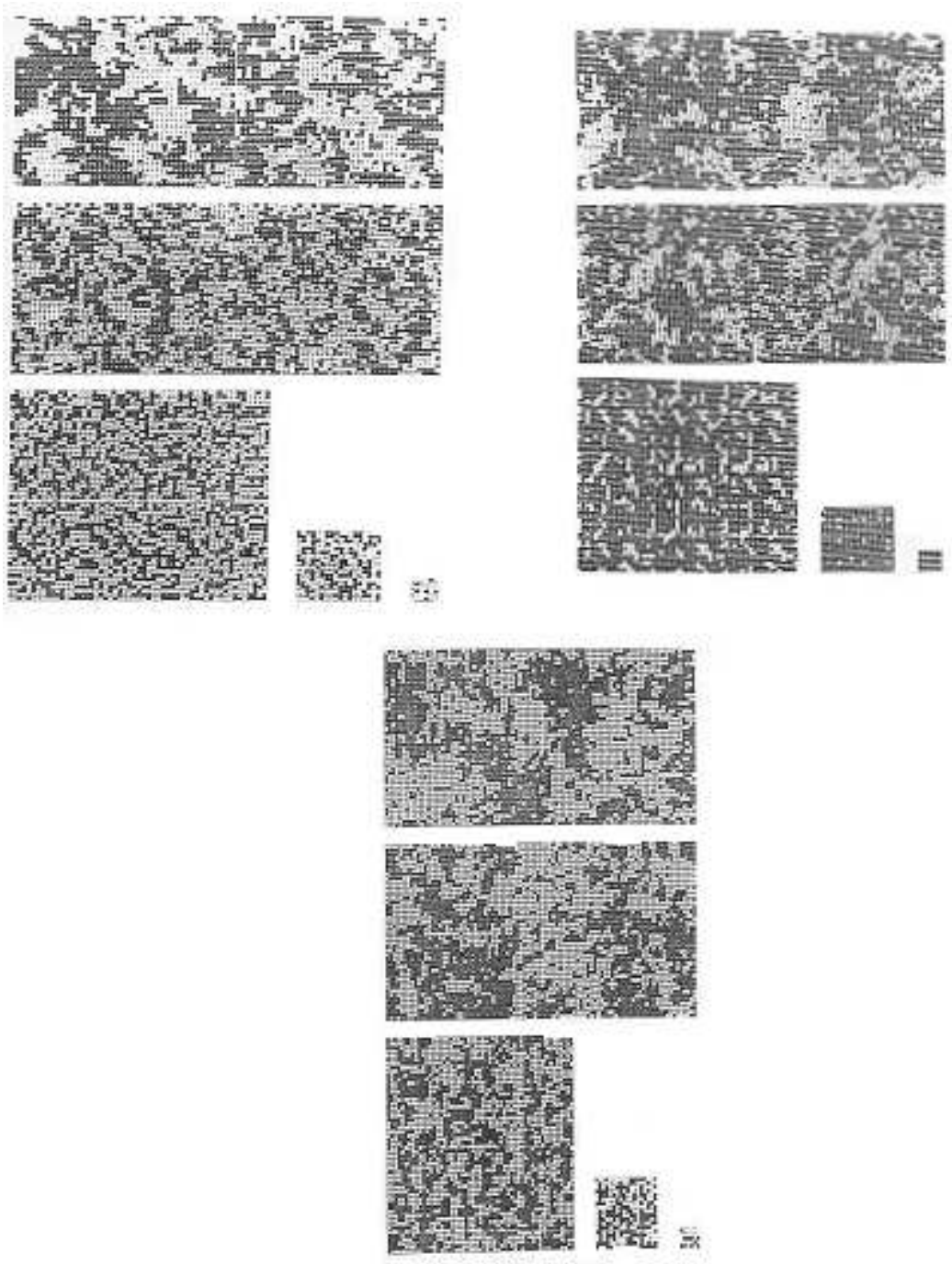

Figure 1.2: A real-space renormalization-group transformation for the two dimensional Ising model on the square lattice. The top-left, top-right, and bottom figures are the renormalization-group flows starting from above, below and on the critical temperature(T_c) respectively. Source: Wilson, K. G. (1979). *Scientific American*, 241, 140.

1.2.1 The Ising Model in One Dimension

The one-dimensional Ising model is a well-known system on which the renormalization-group method can be illustrated. It is defined by the classical Hamiltonian

$$-\beta\mathscr{H} = \sum_{<ij>} Js_is_j + G \equiv \sum_{<ij>} -\beta\mathscr{H}(i,j), \tag{1.7}$$

where J is the interaction coefficient between two nearest-neighbor spins, G is an additive constant and $< ij >$ denotes that the sum is taken over only nearest-neighbor pairs. Every site s_i can take values of $\pm 1/2$. The partition function of the system is

$$Z = \sum_{\{s\}} e^{-\beta\mathscr{H}(s)}. \tag{1.8}$$

Here s represents $\{s_1, s_2, ..., s_{N-1}, s_N\}$, the state of all N spins in the lattice.

In order to implement the renormalization-group procedure we should first decimate(perform the summation over) the odd- (or even-) numbered sites, and then equate the resulting partition function to the original one to find the relation between the renormalized system and the original system. For every cluster of three sites this will give

$$\begin{aligned}
\sum_{s_j=\pm 1/2} e^{-\beta\mathscr{H}(i,j)-\beta\mathscr{H}(j,k)} &= \sum_{s_j=\pm 1/2} e^{-Js_is_j+G+Js_js_k+G} \\
&= \sum_{s_j=\pm 1/2} e^{-Js_j(s_i+s_k)+2G} \\
&= e^{2G}(e^{J(s_i+s_k)/2} + e^{-J(s_i+s_k)/2}) \\
&= e^{J's_is_j+G'} \\
&= e^{-\beta'\mathscr{H}'(i,j)}
\end{aligned} \tag{1.9}$$

defining a renormalized pair Hamiltonian $e^{-\beta'\mathscr{H}'(i,j)}$. At the end, using Eq.(1.9) derived above, a relation between the renormalized interaction coefficients, J', G', and the original coefficients J, G can be found as

$$J' = 2\ln[\cosh(\frac{J}{2})], \quad G' = 2G + \frac{1}{2}\ln[4\cosh(\frac{J}{2})]. \tag{1.10}$$

1.2.2 The Migdal-Kadanoff Procedure

The renormalization-group recursion relations for the regular Ising model and many other classical models in one dimension can be obtained relatively easily by decimating the spins. What is more interesting is to develop a renormalization-group procedure that would be usable to obtain the recursion relations and hence the critical points in higher dimensions. A simple, but very useful, approximate technique is the Migdal-Kadanoff procedure [3]. It makes reasonable predictions for dimensions greater than one which have been helpful in explaining the phase diagrams of real physical systems like krypton adsorbed on graphite [4].

The two steps of the Migdal-Kadanoff procedure on a square lattice are illustrated in Fig.(1.3). First, the bonds of the nearest-neighbor interaction strengths J are moved to create bonds of strength $2J$ at every other line. By repeating the process in both directions symmetry is preserved and we end in a final lattice similar to the first one with bond strengths of $2J$ but with a subset of disconnected sites. Next, the remaining site in the middle of each bond is decimated. Hence, a two-dimensional renormalization is achieved. This idea is important because it makes working in higher dimensions possible. In arbitrary dimensions, any nearest neighbor interaction K_p $(p = 1, 2, ..., d)$ for bonds parallel to the d-axes of a d-dimensional hypercubic lattice can be obtained from

$$K'_p = b^{d-p} R^b (b^{p-1} K_p) \tag{1.11}$$

where R^b is the operator defined by the 1-dimensional decimation and b is the length rescaling factor of the renormalization-group transformation [5].

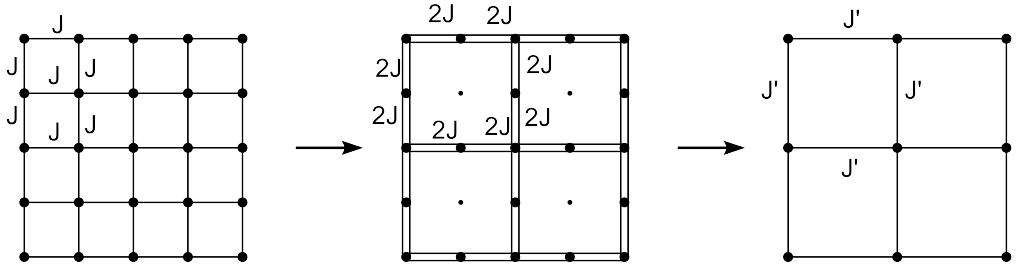

Figure 1.3: Renormalization on a square lattice

2. SYSTEMS WITH QUENCHED RANDOMNESS: BEG SPIN GLASS

2.1 Addition of Randomness

In all of the renormalization-group transformations introduced in the previous chapter, the bonds between sites were all identical to each other. However, any real system is naturally going to contain disorder in it. Although one may wish to get rid of these disordered situations, studying the effects of impurities and randomness on the critical behavior might be exciting. The disorder might lead to new phases in the system, might completely remove the order in the system or sometimes can change the universality class of the system while preserving its order.

The inclusion of some non-magnetic atoms in a lattice consisting of magnetic atoms can be regarded as an example of disorder. In order to create disorder, impurities can be added to a pure material at high temperatures and then the system can be allowed to cool. If this cooling is done sufficiently slowly, the system is going to crystalize, the impurities and the magnetic atoms will come to a thermal equilibrium and the resulting distribution is going to be determined by the final temperature of the system. A disorder obtained in such a way is an example of annealed randomness. If one is going to perform thermodynamic calculations on this system at long time scales, not only the positions of the magnetic ions will be important but also the positions of the impurities will need to be considered. However, the mobility of the impurities is very low in a solid structure and achieving thermal equilibrium might take very long times. It would be more realistic to accept the positions of the impurities as constant and do the calculations only on magnetic degrees of freedom. This would correspond to a quenched random system [6].

One of the important effects of adding randomness to an ordered system might be the appearance of a spin-glass phase which was not present before. The frozen structural disorders which result from the addition of impurities might cause the interactions between the magnetic moments to become frustrated and hence create a spin-glass phase [7]. As the temperature is lowered, no long-range order of the ferromagnetic or antiferromagnetic type will occur but the system is going to have a freezing transition characterized by a new type of order parameter. The physics of spin-glasses raises essential questions and that is why this phenomenon is one of the central research fields in condensed matter physics.

The renormalization-group transformation of a system including quenched randomness can be done through the use of hierarchial lattices [8–10]. In general, a hierarchical lattice can be constructed by replacing every bond in the connected cluster of bonds with the connected cluster of bonds itself and repeating this step infinitely many times. Unique recursion relations can be found for each hierarchial lattice leading to the solutions of the thermodynamic properties of that system.

There are certain interesting questions to be answered related to the effects of randomness on systems. Suppose there exist two phases separated by a phase boundary having first-order and second-order phase transitions meeting on a tricritical point. One might ask how would quenched randomness affect the nature of this phase boundary. It is also worth investigating whether the addition of quenched randomness completely eliminates first-order phase transitions or not, and the way the evolution between phases takes place. In the remaining part of this chapter, the effects of quenched randomness on a complex system are going to be examined and answers will be sought to the questions above.

2.2 The Blume-Emery-Griffiths Spin Glass and Inverted Tricritical Points

One of the attractive systems containing both first- and second-order phase transitions along with tricritical and critical-end point phase diagrams is the Blume-Emery-Griffiths model [11,12]. This system has pure-system tricritical and critical points in $d = 3$. However, the inclusion of quenched randomness increase the interest in this system, as it is predicted that first-order boundaries should thus be converted to second order. In a well-known phase diagram topology,

a tricritical point separates the high-temperature second-order boundary and the low-temperature first-order boundary. In the present work, we find that a temperature sequence of transitions that is reverse to the above can occur with the inclusion of quenched randomness. Thus, an *inverted tricritical point* is obtained, separating a high-temperature first-order boundary and a low-temperature second-order boundary. Interest is further compounded with spin-glass type of quenched randomness [13], as the spin-glass phase appears within the Blume-Emery-Griffiths global phase diagram. Thus, a new spin-glass phase diagram topology was found, in which disconnected spin-glass regions occur close to the ferromagnetic and antiferromagnetic phases, but are separated by a paramagnetic gap.

2.2.1 The Recursion Relations

We have studied, in spatial dimension $d = 3$, the model with Hamiltonian

$$-\beta\mathscr{H} = \sum_{<ij>} [J_{ij}s_i s_j + K s_i^2 s_j^2 - \Delta(s_i^2 + s_j^2)], \tag{2.1}$$

where $s_i = 0, \pm 1$ at each site i of the lattice and $< ij >$ indicates summation over nearest-neighbor pairs of sites. The interaction constants, J, K, Δ, respectively represent the linear exchange coefficient, the quadratic exchange coefficient and the crystal-field interaction. The spin-glass type of quenched randomness is given by each local J_{ij} being ferromagnetic with the value $+J$ with probability $1-p$ and anti-ferromagnetic with the value $-J$ with probability p. With this representation, $p = 0$ and $p = 1$ limits correspond to purely ferromagnetic and purely anti-ferromagnetic systems respectively. Under the scale change induced by renormalization-group transformation, all renormalized interactions become quenched random and the more general Hamiltonian

$$-\beta\mathscr{H} = \sum_{<ij>} [J_{ij}s_i s_j + K_{ij} s_i^2 s_j^2 - \Delta_{ij}(s_i^2 + s_j^2) - \Delta_{ij}^{\dagger}(s_i^2 - s_j^2)] \tag{2.2}$$

has to be considered.

With the quenched randomness added to the system, the renormalization-group transformation is expressed in terms of the joint quenched probability distribution

$P(J_{ij}, K_{ij}, \Delta_{ij}, \Delta_{ij}^{\dagger})$, which is renormalized through the convolution [14]

$$P'(\mathbf{K}'_{i'j'}) = \int [\prod_{ij}^{i'j'} d\mathbf{K}_{ij} P(\mathbf{K}_{ij})] \delta(\mathbf{K}'_{i'j'} - \mathbf{R}(\{\mathbf{K}_{ij}\})), \tag{2.3}$$

where the primes refer to the renormalized system, $\mathbf{K}_{ij} \equiv (J_{ij}, K_{ij}, \Delta_{ij}, \Delta_{ij}^{\dagger})$. $P'(\mathbf{K}_{i'j'})$ in the re-scaled system is calculated from $P'(\mathbf{K}_{ij})$ in the original system so that the product in the integral is over all the bonds ij in the connected cluster of the original system between sites i and j. Here, $\mathbf{R}(\mathbf{K}_{ij})$ is a local recursion relation for each of the bond strengths.

The integral equation is solved numerically using an hierarchical lattice. Hence, we obtain a model solvable by renormalization-group procedure. The probability distribution $P(J, K, \Delta, \Delta^{\dagger})$ is represented by histograms, where each histogram is specified by bond strengths and their corresponding probabilities. For our problem, the initial probability distribution will consist of two histograms; one at $(J, K, \Delta, 0)$ with a probability of $1 - p$ and one at $(-J, K, \Delta, 0)$ with a probability of p. The hierarchial lattice that we studied (Figure 2.1) represents a three-dimensional lattice with a scaling factor of 3, and contains 27 bonds, therefore a direct application of Eq.(2.3) will result in a convolution of 27 probability distributions.

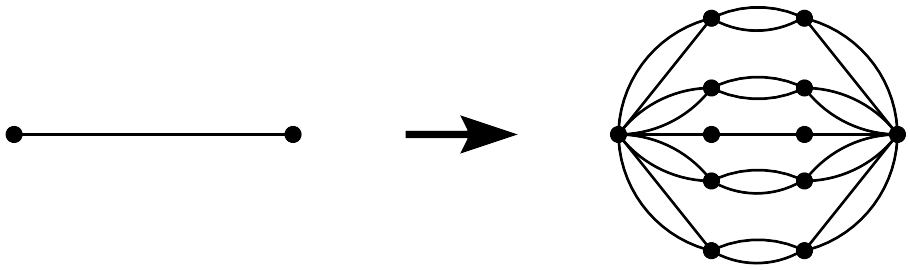

Figure 2.1: The d=3 hierarchial lattice for which our calculation is exact. This lattice is constructed by the repeated imbedding of the graph as shown in this figure. This hierarchical lattice gives very accurate results for the critical temperatures of the $d = 3$ isotropic and anisotropic Ising models. [15]

However, Eq.(2.3) can be separated into pairwise convolutions, each of which having two distributions convoluted at a time using an appropriate R function. The necessary convolutions are a bond moving convolution, with

$$R_{bm}(K_{i1j1} + K_{i2j2}) = K_{i1j1} + K_{i2j2} \tag{2.4}$$

and a decimation convolution yielding the following renormalized interactions:

$$J'_{i'j'} = \ln(R_3/R_4)/2, \qquad K'_{i'j'} = \ln(R_o^2 R_3 R_4/R_1^2 R_2^2)/2,$$
$$\Delta'_{i'j'} = \ln(R_1 R_2/R_o^2)/2, \qquad \Delta^{\dagger\prime}_{i'j'} = \ln(R_1/R_2)/2, \tag{2.5}$$

where

$$R_o = 2\exp(\Delta_{ij} - \Delta^{\dagger}_{jk} + \Delta_{jk} + \Delta^{\dagger}_{jk}) + 1$$

$$\begin{aligned} R_1 = {} & \exp(J_{ij} + K_{ij} + 2\Delta_{ij} + \Delta_{jk} + \Delta^{\dagger}_{jk}) \\ & + \exp(-J_{ij} + K_{ij} + 2\Delta_{ij} + \Delta_{jk} + \Delta^{\dagger}_{jk}) \\ & + \exp(\Delta_{ij} + \Delta^{\dagger}_{ij}), \end{aligned}$$

$$\begin{aligned} R_2 = {} & \exp(\Delta_{ij} - \Delta^{\dagger}_{ij} + J_{jk} + K_{jk} + 2\Delta_{jk}) \\ & + \exp(\Delta_{ij} - \Delta^{\dagger}_{ij} - J_{jk} + K_{jk} + 2\Delta_{jk}) \\ & + \exp(\Delta_{jk} - \Delta^{\dagger}_{jk}), \end{aligned}$$

$$\begin{aligned} R_3 = {} & \exp(J_{ij} + K_{ij} + 2\Delta_{ij} + J_{jk} + K_{jk} + 2\Delta_{jk}) \\ & + \exp(-J_{ij} + K_{ij} + 2\Delta_{ij} - J_{jk} + K_{jk} + 2\Delta_{jk}) \\ & + \exp(\Delta_{ij} + \Delta^{\dagger}_{ij} + \Delta_{jk} - \Delta^{\dagger}_{jk}), \end{aligned}$$

$$\begin{aligned} R_4 = {} & \exp(J_{ij} + K_{ij} + 2\Delta_{ij} - J_{jk} + K_{jk} + 2\Delta_{jk}) \\ & + \exp(-J_{ij} + K_{ij} + 2\Delta_{ij} + J_{jk} + K_{jk} + 2\Delta_{jk}) \\ & + \exp(\Delta_{ij} + \Delta^{\dagger}_{ij} + \Delta_{jk} - \Delta^{\dagger}_{jk}). \end{aligned}$$

For our hierarchial lattice, using the bond-moving and the decimation convolutions, the order of pairwise convolutions yielding the total convolution of equation (2.3) is: (i) a bond moving convolution of $P_{initial}$ with itself, yielding P_1; (ii) a decimation convolution of P_1 with itself yielding P_2; (iii) a decimation convolution of P_2 with P_1 ,yielding P_3; (iv) a bond moving convolution of P_3 with itself, yielding P_4, (v) a bond moving convolution of P_4 with itself, yielding P_5; (vi) a decimation convolution of $P_{initial}$ with itself, yielding P_6; (vii) a decimation convolution of P_6 with $P_{initial}$ yielding P_7; (viii) a bond moving convolution of P_7 with P_5, yielding P_{final}. The number of histograms representing the probability distributions increases rapidly, therefore before every pairwise convolution the number of histograms is controlled at a desired value using a

binning procedure, in a way such that the average and the standard deviations of the probability distributions are preserved. At the end, our results are obtained by the renormalization-group flows of 22,500 histograms. The histograms are placed on a grid of interactions on a four-dimensional interaction space $(J_{ij}, K_{ij}, \Delta_{ij}, \Delta_{ij}^{\dagger})$ and all histograms that fall within the same grid cell are combined together to represent one new interaction point, while the histograms falling outside the grid are grouped together in a single histogram. The size of the grid is adjusted so that only a negligible portion of the histograms will fall outside the grid. Once P_{final} is reached after the 8 piecewise convolutions with a binning step between each of them, P_{final} is re-set as P_{inital} and the same routine is repeated until the characteristics of the flow are fully determined.

2.2.2 Phase Diagrams and Results

Using the recursion relations derived in the previous section it was possible to determine the phase diagram of our system. A detailed study of the calculated phase diagrams, by pinching the phase transition lines, enabled us to observe different kinds of phase transitions between the ferromagnetic and the disordered phases. We have found 3 different kinds of behavior on the phase boundary of ferromagnetic and disordered states as well as a spin-glass phase which was not present before the inclusion of impurities. The first region, corresponding to a second-order phase transition had a sink with a fixed point of $J = 0.184, \Delta/J = -\infty$. Any trajectory, initiated within a narrow neighborhood of this second-order line, will first follow the phase boundary before it reaches the second-order fixed point. Once the flow reaches the fixed point, it is going to stay there for some time (some number of iterations), after which it is going to choose between disordered and ferromagnetic states depending on which side of the phase boundary it was initiated from.

The next region observed was a strong-coupling second-order phase transition region. Flows initiating in this segment of the phase boundary no longer visit the second-order fixed point explained above. Instead, they have their unique fixed distribution. In this strong coupling region, at each renormalization-group iteration, the value of $(2\Delta_{avg} - J_{avg} - K_{avg})$ increases by a factor of 9, hence giving

a critical exponent value of 2 for our $b = 3$, $d = 3$ system, indicating that it is not a first-order transition. Finally, we observed a first-order phase transition region in which the critical exponent was found to be 3, which is equal to d, and the first-order phase transition criterion for our system is satisfied.

Tricritical phase diagram cross-sections of the purely ferromagnetic system for different K/J values are shown in Fig.2.2. These are standard tricritical phase diagrams, in the absence of quenched randomness, with the tricritical point separating the second-order transitions at high temperature and the first-order transitions at low temperature. The humped boundary, occurring in mean-field theory but not in the $d = 2$ system [12], is thus found to occur in the $d = 3$ system.

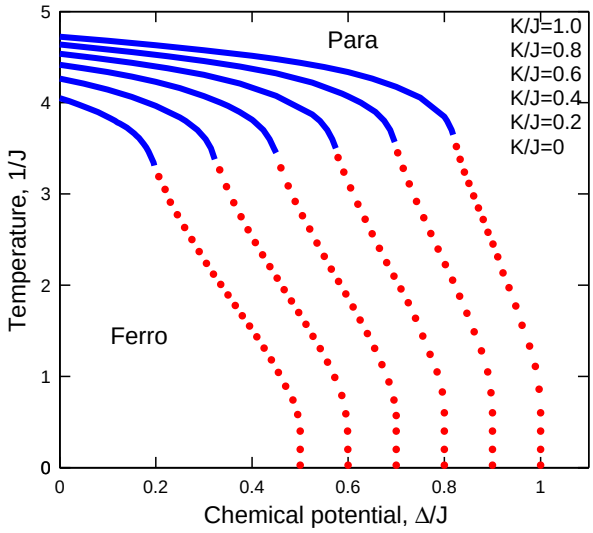

Figure 2.2: Tricritical phase diagram cross-sections of the purely ferromagnetic system for different K/J values, shown consecutively from the innermost curve for $K/J = 0$. First- and second-order transitions are respectively shown by dotted and full lines, meeting at a tricritical point. In these systems, with no quenched randomness, the standard tricritical topology occurs, with the second-order boundary at high temperature and the first-order boundary at low temperature.

Our calculated global phase diagram for the BEG spin-glass system is in Fig.2.3 for $K = 0$. The ferromagnetic phase is bounded by a first-order surface close to $p = 0$, which recedes along the full line on the surface from a new second-order transition induced by randomness and controlled by a strong-coupling fixed distribution. At the dashed line, an ordinary second-order transition takes over. The full line is thus a line of random-bond tricritical points. The dashed line

is a line of special critical points around which universality is violated, since the second-order phase transitions on each side of this line have different critical exponents. [14] These two lines meet at the non-random ($p = 0$) tricitical point. The transitions from the spin-glass phase, to the paramagnetic or ferromagnetic phase, are second order.

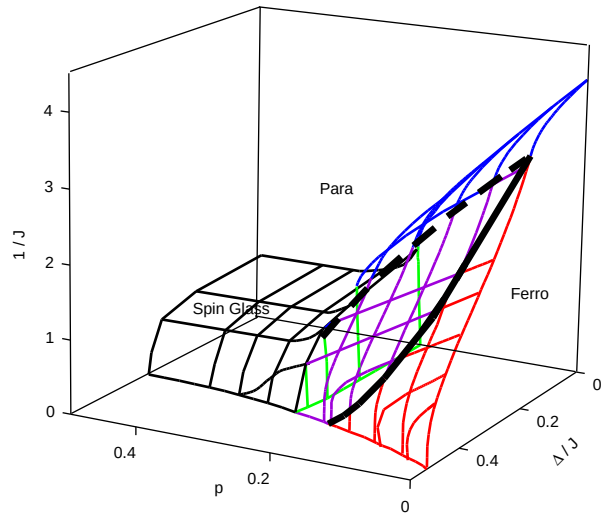

Figure 2.3: Our calculated global phase diagram for $K = 0$. The ferromagnetic phase is bounded by a first-order surface close to $p = 0$, which recedes along the full line on the surface from a new second-order transition induced by randomness and controlled by a strong-coupling fixed distribution. At the dashed line, an ordinary second-order transition takes over. The transitions from the spin-glass phase, to the paramagnetic or ferromagnetic phase, are second order. The system being symmetric about $p = 0.5$, the antiferromagnetic sector is not shown.

Cross-sections of this global phase diagram for constant chemical potential Δ/J of the non-magnetic state are in Fig.2.4. The outermost cross-section has $\Delta/J = -\infty$, meaning no $s_i = 0$ states, and therefore is equivalent to the phase diagram of the spin-1/2 Ising spin glass [16], showing as temperature is lowered the paramagnet-ferromagnet-spinglass reentrance [17, 18]. The annealed vacancies, namely the nonmagnetic states $s_i = 0$, are introduced in cross-sections with successively higher values of Δ/J. For Δ/J greater than the non-random tricritical value of $\Delta/J = 0.192$, first-order transitions between the ferromagnetic and paramagnetic phases are introduced from the low randomness side, but are converted to the strong-coupling second-order transition at a threshold value of randomness p. This constitutes an *inverted tricritical point*, since the phase boundary is converted from first order to second order as temperature

is lowered, contrary to the ordinary tricritical points (as seen for example in Fig.2.2). The above results are consistent with the general prediction that, in $d = 3$, quenched randomness gradually converts first-order boundaries into second order. [19] (In $d = 2$, this conversion is predicted to happen with infinitesimal quenched randomness. [19, 20]). As the annealed vacancies $s_i = 0$ are increased,

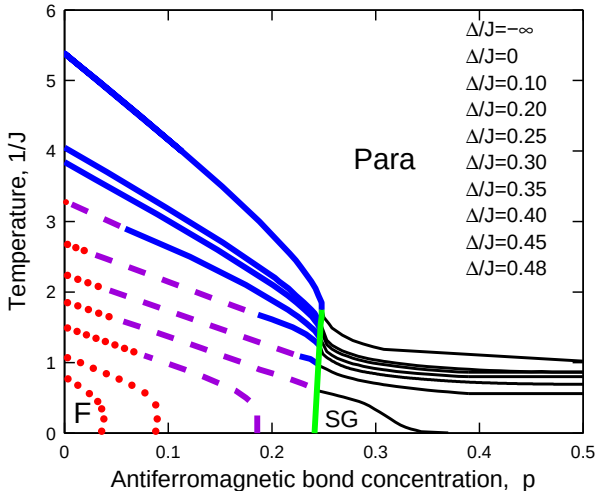

Figure 2.4: Blume-Emery-Griffiths spin-glass phase diagrams: Constant Δ/J cross-sections of the global phase diagram in Fig.1. The outermost cross-section has $\Delta/J = -\infty$, meaning no $s_i = 0$ states. The annealed vacancies $s_i = 0$ are introduced in cross-sections with successively higher values of Δ/J, making all ordered phases recede. The dotted and full lines are respectively first- and second-order phase boundaries. The dashed lines are strong-coupling second-order phase boundaries induced by quenched randomness. The inverted tricritical topology is seen between the dotted and dashed lines, with the first-order transitions occurring at high temperature and the second-order transitions occurring at low temperature, on each side of the tricritical point. A new phase spin-glass phase diagram topology is obtained for $\Delta/J = 0.35$, in which the spin-glass phase occurs close to the ferromagnetic (and, symmetrically, antiferromagnetic, not shown here) phase, but yields to the paramagnetic phase as p is increased towards 0.5. The spin-glass phase disappears at $\Delta/J = 0.37$.

at $\Delta/J \geq 0.34$, of the second-order transitions between the ferromagnetic and paramagnetic phases, only the strong-coupling transition remains. At $\Delta/J \geq 0.42$, the strong-coupling second-order transition also disappears, leaving only first-order transitions between the ferromagnetic and paramagnetic phases. Also as the annealed vacancies are increased, all ordered phases recede. In this process, first the spin-glass phase disappears, at $\Delta/J = 0.37$, which is understandable, since it is tenuously ordered due to frustration. The new, *disconnected spin-glass* phase

diagram topology is obtained in this neighborhood, e.g., for $\Delta/J = 0.35$ as shown in Fig.2.4, in which the spin-glass phase occurs close to the ferromagnetic (and, symmetrically, antiferromagnetic, not shown in the figures) phase, but yields to the paramagnetic phase as p is increased towards 0.5 .

The paramagnetic-ferromagnetic-spin-glass reentrances, as temperature is lowered, of the Blume-Emery-Griffiths spin-glass cross-sections fall on the same reentrant second-order boundary, as seen in Fig.2.4. As seen for $\Delta/J = 0.45$ and 0.48 in this figure, before disappearing at $\Delta/J = 0.5$, the ferromagnetic phase exhibits paramagnetic-ferromagnetic-paramagnetic reentrance as temperature is lowered.

Constant p cross-sections of the global phase diagram in Fig.2.3 are shown in Fig.2.5. The outermost curve corresponds to the pure Blume-Emery-Griffiths model with no quenched randomness ($p = 0$). As spin-glass quenched randomness is introduced with increasing values of p, we see that the first-order boundary recedes to the strong-coupling second-order boundary, while the ordinary second-order boundary also expands. At $p = 0.18$, the first-order transition completely disappears. At $p = 0.241$, the spin-glass phase appears below the ferromagnetic phase, reflecting complete reentrance. At $p = 0.249$, the spin-glass phase completely replaces the ferromagnetic phase as the ordered phase, which is enveloped by second-order transitions only. Thus, for $0.241 < p < 0.759$, the second-order boundary between the spin-glass and paramagnetic phases reaches zero temperature.

In the results above, the phase diagrams are determined by the basins of attraction of the renormalization-group sinks, namely the completely stable fixed points and fixed distributions: Each basin is a thermodynamic phase. The nature of the phase transitions is determined by analysis of the unstable fixed points and fixed distributions to which the phase diagram points of these transitions flow. Fig.2.6 shows the unstable fixed distributions of (a) the quenched randomness-induced second-order transitions between the ferromagnetic and paramagnetic phases, (b) the first-order transitions between the ferromagnetic and paramagnetic phases, (c) the second-order transitions between the ferromagnetic and spin-glass phases, and (d) the second-order transitions between the spin-glass and paramagnetic phases.

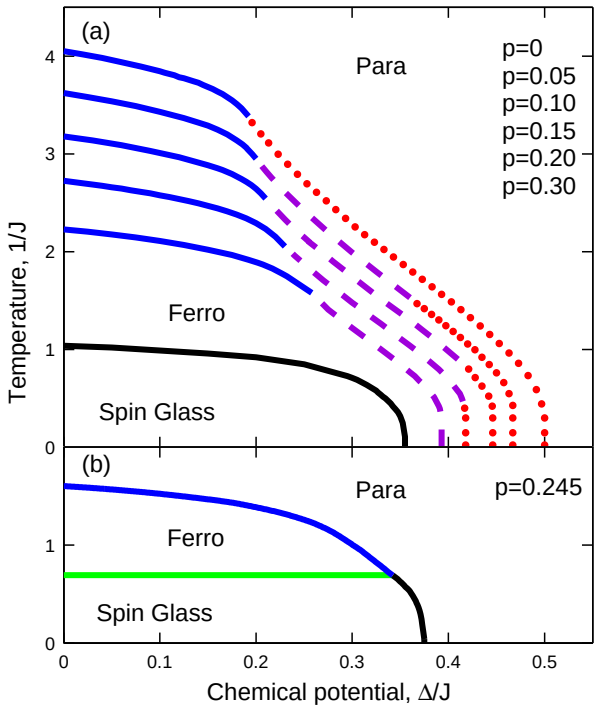

Figure 2.5: Spin-glass Blume-Emery-Griffiths phase diagrams: Constant p cross-sections of the global phase diagram in Fig.1. The dotted and full lines are respectively first- and second-order phase boundaries. The dashed lines are strong-coupling second-order phase boundaries induced by quenched randomness. The outermost curve corresponds to the pure Blume-Emery-Griffiths model with no quenched randomness $(p = 0)$. As spin-glass quenched randomness is introduced with increasing values of p, ordered phases and first-order phase transitions recede.

The (totally stable) sink fixed distribution of the spin-glass phase is also shown, in (e). The eigenvalue exponent of the unstable fixed distribution controlling (b) the first-order transitions between the ferromagnetic and paramagnetic phases is $y = 3 = d$, as is required for first-order transitions. The eigenvalue exponents of the other unstable fixed distributions, (a),(c),(d), are $y < d$ as is required for second-order transitions.

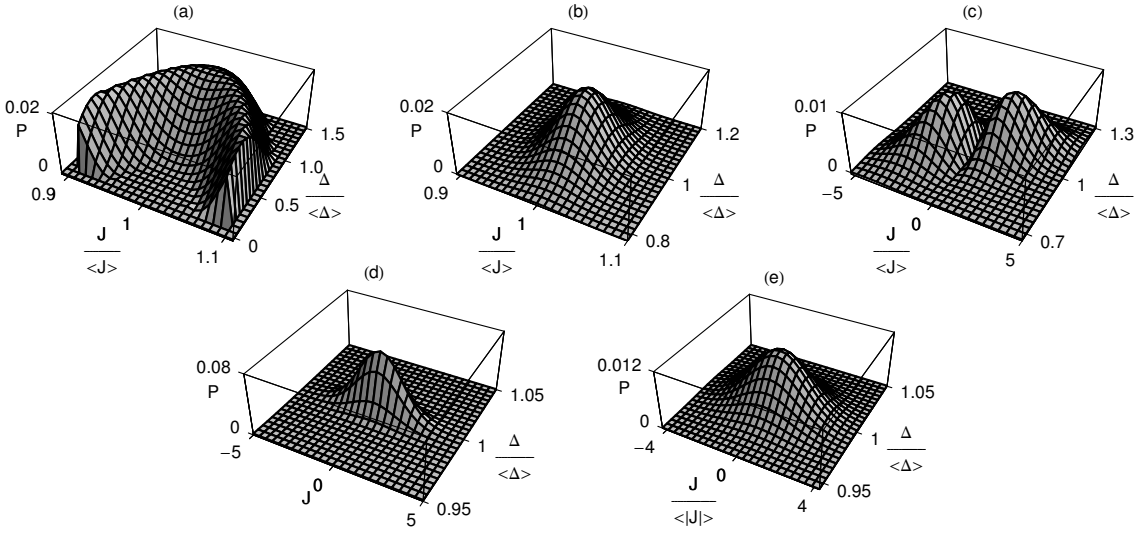

Figure 2.6: Projections of the fixed distributions $P^*(J_{ij}, K_{ij}, \Delta_{ij}, \Delta_{ij}^\dagger)$ for: (a) the disorder-induced second-order transitions between the ferromagnetic and paramagnetic phases, (b) the first-order transitions between the ferromagnetic and paramagnetic phases, (c) the second-order transitions between the ferromagnetic and spin-glass phases, (d) the second-order phase transitions between the spin-glass and paramagnetic phases, and (e) the sink fixed distribution for the spin-glass phase. Note that (a),(b),(c),(e) are runaways, in the sense that the couplings renormalize to infinity while the distribution retains its shape shown here. In the second-order phase transitions between the spin-glass and paramagnetic phases (d), Δ is a runaway (to minus infinity), while the other interactions remain finite. The fixed distributions in this figure are singly unstable, except for the sink (e), which is totally stable.

3. PHASE TRANSITIONS IN QUANTUM SYSTEMS

All systems in nature obey quantum mechanics. The study of phase transitions in fermionic and bosonic systems has been one of the most interesting aspects of quantum systems since it involves numerous exciting effects like superconductivity [21], the metal-insulator transition [22], metallic magnetism [23], heavy fermion behavior [24, 25], ferromagnetism, anti-ferromagnetism, etc. Although most earlier studies had focused on zero-temperature behavior, with the discovery of the high-temperature superconducting ceramics [26] increasing attention has been given to finite-temperature studies of phase transitions in quantum systems of interacting electrons. The natural starting point for a theory of high-T_c materials is to write down a Hamiltonian modeling the behaviors of the electrons in the system of interest. The Hubbard model is a simple but realistic model for describing electronic systems. In this chapter, as a first step toward more complicated systems, applications of renormalization-group theory to spinless fermionic and bosonic Hubbard models will be presented.

3.1 The Hubbard Model with Spinless Fermions

The Hubbard model we examined is defined by the Hamiltonian

$$-\beta\mathscr{H} = -t\sum_{<ij>}(c_i^\dagger c_j + c_j^\dagger c_i) + \mu\sum_{<ij>}(n_i + n_j) - U\sum_{<ij>} n_i n_j + \sum_{<ij>} G \qquad (3.1)$$

with $\beta = 1/kT$. The terms in the Hamiltonian are the kinetic energy term (parameterized by the electron hopping strength t), the nearest neighbor attraction term ($U < 0$) and the chemical potential μ_0. Here $c_i^\dagger$ and c_i represent respectively the creation and destruction operators obeying the anticommutation rules for a fermionic system, $\{c_i, c_j^\dagger\} = \delta_{ij}$, and the commutation rules for a bosonic system, $[c_i, c_j^\dagger] = \delta_{ij}$.

3.1.1 Derivation of the Recursion Relations

The general Hamiltonian given in Eq.(3.1) can be written as

$$-\beta\mathscr{H} = \sum_i [-\beta\mathscr{H}(i,i+1)], \tag{3.2}$$

where $-\beta H(i,i+1)$ is the Hamiltonian of a neighboring pair on the lattice. The decimation procedure that was used for the classical system studied in Chapter 2 is of no use for the quantum system because the exponential of the sum of pair Hamiltonians can no longer be expressed as a product of the individual exponentiated Hamiltonians. Therefore, summing over the 'middle' terms in order to eliminate half of the sites is done approximately by using the Suzuki-Takano approximation [27, 28]:

$$\begin{aligned}
\mathrm{Tr}_{even} e^{-\beta\mathscr{H}} &= \mathrm{Tr}_{even} e^{\Sigma_i \{-\beta\mathscr{H}(i,i+1)\}} \\
&= \mathrm{Tr}_{even} e^{\Sigma_i^{even} \{-\beta\mathscr{H}(i-1,i)-\beta\mathscr{H}(i,i+1)\}} \\
&\simeq \prod_i^{even} Tr_i e^{\{-\beta\mathscr{H}(i-1,i)-\beta\mathscr{H}(i,i+1)\}} \\
&= \prod_i^{even} e^{-\beta'\mathscr{H}'(i-1,i+1)} \\
&\simeq e^{\Sigma_i^{even} \{-\beta'\mathscr{H}'(i-1,i+1)\}} \\
&= e^{-\beta'\mathscr{H}'}.
\end{aligned} \tag{3.3}$$

In the above derivation, the non-commutation of operators separated beyond three consecutive sites of the unrenormalized system was ignored. Since in both of the approximation steps the same approach was used in opposite directions, one can expect a compensation of errors. Note that we have implemented

$$e^{-\beta\mathscr{H}_1-\beta\mathscr{H}_2} = e^{-\beta\mathscr{H}_1} e^{-\beta\mathscr{H}_2} e^{C} \tag{3.4}$$

where the correction term, $C = \beta^2[\mathscr{H}1, \mathscr{H}2] + \textit{higher order terms}$, is going to vanish as $\beta \to 0$ or $T \to \infty$. Therefore, our approximation becomes exact at high temperatures. Earlier studies have verified the success of this approximation at predicting the finite temperature behaviors of quantum spin systems [27, 28].

From the above derivation, Eq.(3.3), the renormalized pair Hamiltonian $-\beta'\mathscr{H}'(i,j)$ can be extracted as:

$$e^{-\beta'\mathscr{H}'(i-1,i+1)} = \mathrm{Tr}_i e^{-\beta\mathscr{H}(i-1,i)-\beta\mathscr{H}(i,i+1)}. \tag{3.5}$$

Eq.(3.5) is an operator equality and by choosing an appropriate basis it can be written as a matrix equality as follows:

$$\langle u_i v_k | e^{-\beta' \mathscr{H}'(i,k)} | \overline{u}_i \overline{v}_k \rangle = \sum_{w_j} \langle u_i w_j v_k | e^{-\beta \mathscr{H}(i-1,i) - \beta \mathscr{H}(i,i+1)} | \overline{u}_i \overline{w}_j \overline{v}_k \rangle. \tag{3.6}$$

Here, u,v and w are sites which can be either empty ($\circ$) or occupied ($\bullet$). Now the strategy of solving the system will be to find the matrix elements on both sides of Eq.(3.6), and then to contract the right-hand side to the left-hand side matrix to obtain the recursion relations of the system. The unrenormalized 8×8 Hamiltonian matrix, the right hand side of Eq. (3.6) was found as:

	$\lvert\circ\circ\circ\rangle$	$\lvert\bullet\circ\circ\rangle$	$\lvert\circ\bullet\circ\rangle$	$\lvert\circ\circ\bullet\rangle$	$\lvert\bullet\bullet\circ\rangle$	$\lvert\bullet\circ\bullet\rangle$	$\lvert\circ\bullet\bullet\rangle$	$\lvert\bullet\bullet\bullet\rangle$
$\langle\circ\circ\circ\rvert$	0	0	0	0	0	0	0	0
$\langle\bullet\circ\circ\rvert$	0	μ	$-t$	0	0	0	0	0
$\langle\circ\bullet\circ\rvert$	0	$-t$	2μ	$-t$	0	0	0	0
$\langle\circ\circ\bullet\rvert$	0	0	$-t$	μ	0	0	0	0
$\langle\bullet\bullet\circ\rvert$	0	0	0	0	$-U+3\mu$	$-t$	0	0
$\langle\bullet\circ\bullet\rvert$	0	0	0	0	$-t$	2μ	$-t$	0
$\langle\circ\bullet\bullet\rvert$	0	0	0	0	0	$-t$	$-U+3\mu$	0
$\langle\bullet\bullet\bullet\rvert$	0	0	0	0	0	0	0	$-2U+4\mu$

For calculational purposes, the matrices of Eq.(3.6) were diagonalized by using the basis states $\{|\Phi_p\rangle\}$ and $\{|\Psi_q\rangle\}$, which are shown in Table(3.1) with their corresponding eigenvalues. With these states, Eq.(3.6) can be re-written as

$$\begin{aligned} \gamma_p &\equiv \langle \phi_p | e^{-\beta' H'(i,k)} | \phi_p \rangle \qquad (3.7) \\ &= \sum_{u,v,\overline{u},\overline{v},w,q} \langle \phi_p | u_i v_k \rangle \langle u_i w_j v_k | \psi_q \rangle \langle \psi_q | e^{-\beta H(i,j) - \beta H(j,k)} | \psi_q \rangle \langle \psi_q | \overline{u}_i w_j \overline{v}_k \rangle \langle \overline{u}_i \overline{v}_k | \phi_p \rangle \end{aligned}$$

Using the four γ_p values obtained from Eq.(3.7), the recursion relations giving the renormalized coefficients G',t',μ',U' were theoretically calculated for a $b = 2$

system in 3 dimensions as

$$\begin{aligned} G' &= 8G + 4\ln\gamma_1, \\ t' &= 2\ln\frac{\gamma_3}{\gamma_2}, \\ \mu' &= 2\big(\ln(\gamma_3\gamma_2) - 2\ln\gamma_1\big), \\ U' &= 4\big[\ln\big(\frac{\gamma_2\gamma_3}{\gamma_4}\big) - \ln\gamma_1\big], \end{aligned} \tag{3.8}$$

where

$$\begin{aligned} \gamma_1 &= 1 + \frac{e^{\frac{1}{2}(3\mu-\sqrt{\mu^2+8t^2})}\big(\mu-\sqrt{\mu^2+8t^2}\big)^2}{4t^2\Big(2+\frac{1}{4}\big|\frac{\mu-\sqrt{\mu^2+8t^2}}{t}\big|^2\Big)} + \frac{e^{\frac{1}{2}(3\mu+\sqrt{\mu^2+8t^2})}\big(\mu+\sqrt{\mu^2+8t^2}\big)^2}{4t^2\Big(2+\frac{1}{4}\big|\frac{\mu+\sqrt{\mu^2+8t^2}}{t}\big|^2\Big)}, \\ \gamma_2 &= \frac{2e^{\frac{1}{2}(3\mu-\sqrt{\mu^2+8t^2})}}{2+\frac{1}{4}\big|\frac{\mu-\sqrt{\mu^2+8t^2}}{t}\big|^2} + \frac{2e^{\frac{1}{2}(3\mu+\sqrt{\mu^2+8t^2})}}{2+\frac{1}{4}\big|\frac{\mu+\sqrt{\mu^2+8t^2}}{t}\big|^2} \\ &\quad + \frac{2e^{\frac{1}{2}(5\mu-U-\sqrt{\mu^2+8t^2-2\mu U+U^2})}}{2+\frac{1}{4}\big|\frac{-\mu+U-\sqrt{\mu^2+8t^2-2\mu U+U^2}}{t}\big|^2} + \frac{2e^{\frac{1}{2}(5\mu-U+\sqrt{\mu^2+8t^2-2\mu U+U^2})}}{2+\frac{1}{4}\big|\frac{-\mu+U+\sqrt{\mu^2+8t^2-2\mu U+U^2}}{t}\big|^2}, \\ \gamma_3 &= e^{\mu} + e^{3\mu-U}, \\ \gamma_4 &= e^{4\mu-2U} \\ &\quad + \frac{e^{\frac{1}{2}\left(5\mu-U-\sqrt{m^2+8t^2-2\mu U+U^2}\right)}\Big(-\mu+U-\sqrt{\mu^2+8t^2-2\mu U+U^2}\Big)^2}{4t^2\Big(2+\frac{1}{4}\big|\frac{-\mu+U-\sqrt{\mu^2+8t^2-2\mu U+U^2}}{t}\big|^2\Big)} \\ &\quad + \frac{e^{\frac{1}{2}\left(5\mu-U+\sqrt{\mu^2+8t^2-2\mu U+U^2}\right)}\Big(-\mu+U+\sqrt{\mu^2+8t^2-2\mu U+U^2}\Big)^2}{4t^2\Big(2+\frac{1}{4}\big|\frac{-\mu+U+\sqrt{\mu^2+8t^2-2\mu U+U^2}}{t}\big|^2\Big)}. \end{aligned} \tag{3.9}$$

Table 3.1: The eigenvectors (shown here without normalization factors) used to diagonalize the matrices in Eq.(3.4) and their corresponding eigenvalues. The coefficients appearing in the table are: $C_{26} = \frac{(\mu-U)-\sqrt{(\mu-U)^2+8t^2}}{2t}$, $C_{36} = \frac{(\mu-U)+\sqrt{(\mu-U)^2+8t^2}}{2t}$, $C_{43} = \frac{-\mu-\sqrt{\mu^2-8t^2}}{2t}$, and $C_{53} = \frac{-\mu+\sqrt{\mu^2+8t^2}}{2t}$.

Eigenvector	Eigenvalue
$\|\Psi_1\rangle = -\|\bullet\circ\circ\rangle + \|\circ\circ\bullet\rangle$	$\lambda_1 = \mu$
$\|\Psi_2\rangle = \|\bullet\bullet\circ\rangle + \|\circ\bullet\bullet\rangle$ $+C_{26}\|\bullet\circ\bullet\rangle$	$\lambda_2 = \frac{(5\mu-2U)+\sqrt{(m-U)^2+8t^2}}{2}$
$\|\Psi_3\rangle = \|\bullet\bullet\circ\rangle + \|\circ\bullet\bullet\rangle$ $+C_{36}\|\bullet\circ\bullet\rangle$	$\lambda_3 = \frac{(5\mu-2U)-\sqrt{(m-U)^2+8t^2}}{2}$
$\|\Psi_4\rangle = \|\bullet\circ\circ\rangle + \|\circ\circ\bullet\rangle$ $+C_{43}\|\circ\bullet\circ\rangle$	$\lambda_4 = \frac{3\mu+\sqrt{\mu^2+8t^2}}{2}$
$\|\Psi_5\rangle = \|\bullet\circ\circ\rangle + \|\circ\circ\bullet\rangle$ $+C_{53}\|\circ\bullet\circ\rangle$	$\lambda_5 = \frac{3\mu-\sqrt{\mu^2+8t^2}}{2}$
$\|\Psi_6\rangle = -\|\bullet\circ\bullet\rangle + \|\circ\bullet\bullet\rangle$	$\lambda_6 = -U+3\mu$
$\|\Psi_7\rangle = -\|\bullet\bullet\bullet\rangle$	$\lambda_7 = -2U+4\mu$
$\|\Psi_8\rangle = -\|\circ\circ\circ\rangle$	$\lambda_8 = 0$
$\|\phi_1\rangle = -\|\circ\circ\rangle$	$\Lambda_1 = 0$
$\|\phi_2\rangle = \|\bullet\circ\rangle + \|\circ\bullet\rangle$	$\Lambda_2 = \mu - t$
$\|\phi_3\rangle = \|\bullet\circ\rangle - \|\circ\bullet\rangle$	$\Lambda_3 = \mu + t$
$\|\phi_4\rangle = -\|\bullet\bullet\rangle$	$\Lambda_4 = 2\mu - U$

3.1.2 Calculation of Densities with the Recursion Matrix

If we define an interaction vector $\mathbf{K}$, then each interaction constant K_α present in the Hamiltonian is going to be a coefficient of one of the operators in the original Hamiltonian and we can calculate the expectation values of those operators by using the following procedure. A recursion matrix, whose elements are the derivatives of the recursion relations, will be calculated at each renormalization step until a sink is reached. Through this method, the densities for all of the interaction constants can be found.

For the Hamiltonian of our system, the recursion matrix has the form:

$$\hat{T} = \begin{pmatrix} \frac{\partial G'}{\partial G} & \frac{\partial G'}{\partial t} & \frac{\partial G'}{\partial \mu} & \frac{\partial G'}{\partial U} \\ \frac{\partial t'}{\partial G} & \frac{\partial t'}{\partial t} & \frac{\partial t'}{\partial \mu} & \frac{\partial t'}{\partial U} \\ \frac{\partial \mu'}{\partial G} & \frac{\partial \mu'}{\partial t} & \frac{\partial \mu'}{\partial \mu} & \frac{\partial \mu'}{\partial U} \\ \frac{\partial U'}{\partial G} & \frac{\partial U'}{\partial t} & \frac{\partial U'}{\partial \mu} & \frac{\partial U'}{\partial U} \end{pmatrix}. \tag{3.10}$$

The thermodynamic densities are calculated from

$$\begin{aligned} M_\alpha &= \frac{1}{N}\frac{\partial}{\partial K_\alpha} lnZ \\ &= \frac{1}{N}(\frac{\partial}{\partial K'_\beta} lnZ)\frac{\partial K'_\beta}{\partial K_\alpha} \\ &= b^{-d}\frac{1}{N'}(\frac{\partial}{\partial K'_\beta} lnZ)\frac{\partial K'_\beta}{\partial K_\alpha} \\ &= b^{-d} M'_\beta \frac{\partial K'_\beta}{\partial K_\alpha} \\ &= b^{-d} M'_\beta T_{\beta\alpha} \end{aligned} \tag{3.11}$$

where $\vec{K} = (t, \mu, U, G)$, N is the number of bonds and Z is the partition function. The interaction coefficients, (t, μ, U, G), are not going to change at the fixed points with repeating renormalization steps. Therefore, the equality derived in Eq.(3.11) will become a solvable eigenvalue/eigenvector equality,

$$b^d \vec{M}^* = \vec{M}^* \cdot T^{(k)}. \tag{3.12}$$

Here, $\vec{M}^*$ is the left eigenvector of the recursion matrix $T^{(k)}$ at the fixed point reached after k renormalization steps, with an eigenvalue of b^d. After finding $\vec{M}^*$, repeated applications of Eq.(3.11) allow us to calculate $\vec{M}$ for the original system.

3.1.3 Phase Diagrams and Densities

Using the derived recursion relations, the phase diagrams of the system were calculated. It can be seen from Fig.(3.1) that the system can exist in four different phases: the dilute phase (phase I), the dense phase (phase IV), and two intermediate phases (phase II and phase III) characterized by significant electron hopping. The values of the interaction constants at the phase sinks are shown in Table(3.2). In order to identify the order of the phase transitions, the eigenvalue exponents were calculated at the phase boundaries and it was found that all of the phase transitions for this system are second order (Table 3.3).

Table 3.2: Values of the interaction coefficients at the phase sinks.

Phase No	t	μ	U	μ/t	U/t	U/μ	$\mu-t$	$U-2t$	$\mu+t-U$
I	0	$-\infty$	0	$-\infty$	0	0	$-\infty$	0	$-\infty$
II	$-\infty$	$-\infty$	$-\infty$	1	0	0	2.1126	∞	$-\infty$
III	$-\infty$	$-\infty$	$-\infty$	-1	0	0	∞	∞	-2.1126
IV	0	∞	0	∞	0	0	∞	0	∞

Table 3.3: Values of the interaction coefficients at the phase boundary fixed points and their eigenvalue exponents

Boundary	t	μ	U	μ/t	U/t	U/μ	$\mu-t$	$U-2t$	$\mu+t-U$	Eigenvalue exponents
I - II	$-\infty$	$-\infty$	$-\infty$	1	0	0	1.744	∞	$-\infty$	0.27 , -1.00, $-\infty$
II - III	$-\infty$	$-\infty$	$-\infty$	1	2	2	5.538	11.076	-5.538	0.42 , -1.00, $-\infty$
III -IV	$-\infty$	∞	$-\infty$	-1	0	0	∞	∞	1.744	0.27 , -0.58, $-\infty$
I- IV	0	0	0	0	0	2	0	0	0	2.00, $-\infty$,$-\infty$
Multicritical point	-0.554	-0.034	-0.068	0.062	0.123	2	0.520	1.040	-0.520	1.92,0.776

It can be seen from the phase diagrams that the system exhibits a character which is totally symmetric about the $\frac{\mu}{t} = (\frac{1}{2})\frac{U}{t}$ line, on the plane of $\frac{1}{t}$ vs $\frac{\mu}{t}$. For all the different $\frac{U}{t}$ values, the dilute phase only exists when $\frac{\mu}{t} < 1$ and the dense phase only exists when $\frac{\mu}{t} > 1$. As $\frac{U}{t}$ decreases (leading to a more attractive system), the dense phase expands towards lower $\frac{\mu}{t}$ values and reduces the area of intermediate phases leaving less room for hopping. The intermediate phases, II and III, are seen between the dense and dilute phases for $\frac{U}{t} > -2$ but they disappear with

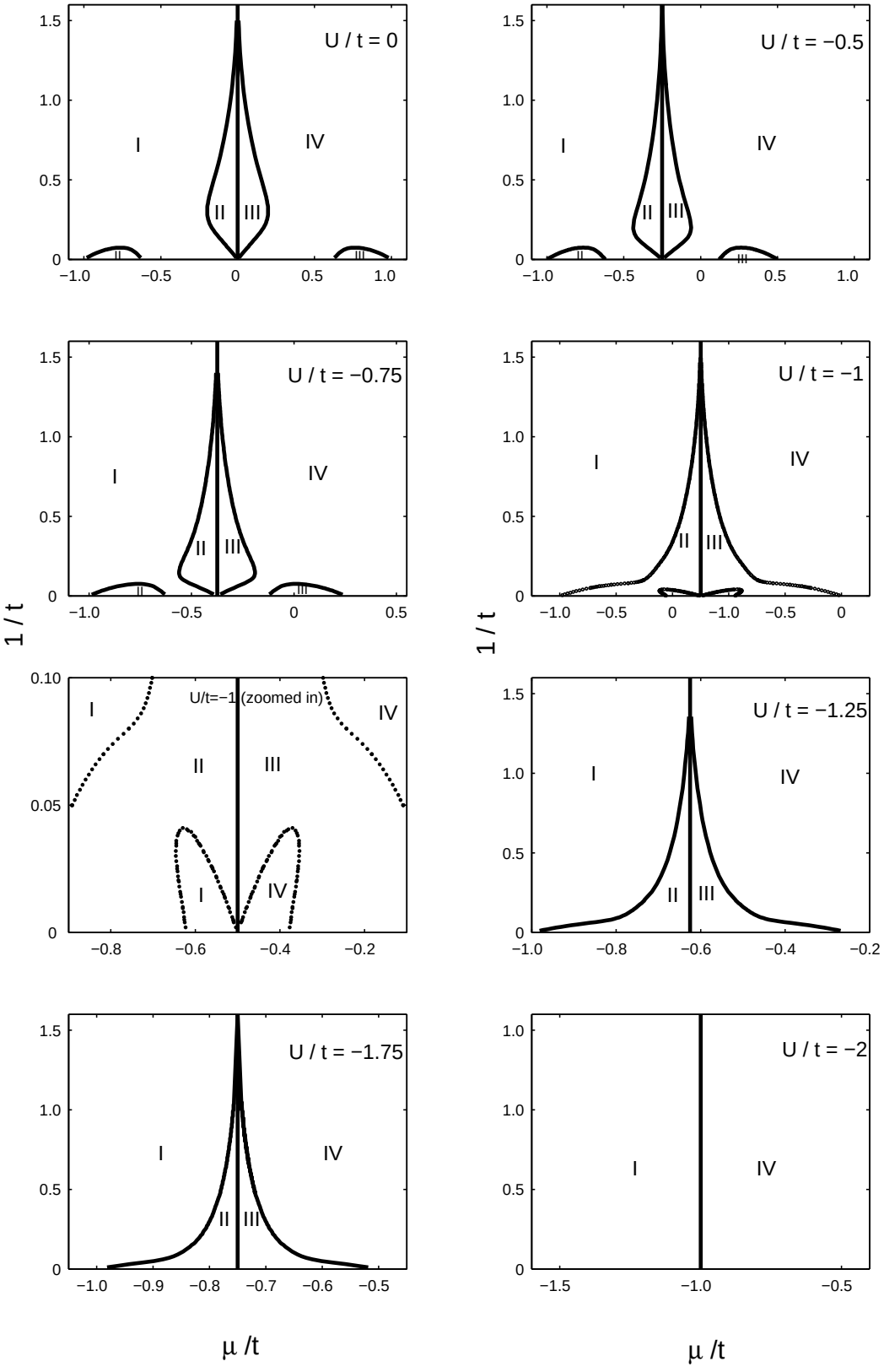

Figure 3.1: Phase diagrams of the fermionic Hubbard model for different U/t values.

decreasing $\frac{U}{t}$ eventually leaving behind only the dilute and dense phases separated by $\frac{\mu}{t} = \frac{U}{2t}$, the vertical boundary. At low $\frac{1}{t}$ values, when $\frac{U}{2t} > -0.63$, phases I and IV (or II and III) reappear in the regions of phase II and III (or phase I and IV) in small islands.

The density diagrams of the t,U, μ terms for different $1/t$ values with $U/t = 1$ are shown in Fig.(3.2-3.5). It can be seen from the diagrams that for high values of μ/t, all sites get filled completely and no hopping exists as predicted for a dense phase. Similarly there is no hopping for low μ/t values since all sites are empty in that region as predicted for a dilute phase. The hopping of particles takes place mostly in the intermediate phase regions (Table 3.4). In the diagrams, the full line represents the hopping density $< c_i^\dagger c_j + c_j^\dagger c_i >$, the dashed line represents $< n_i + n_j >$ and the dotted line represents $< n_i n_j >$. The vertical dashed lines correspond to the phase transitions. It should be noted that close to the phase transition regions, there is an increase in the slopes of $< n_i + n_j >$ and $< n_i n_j >$ as a function of μ/t, particularly for low $1/t$.

Table 3.4: Expectation values at the phase sinks.

Phase No	$\langle$ hopping $\rangle$	$\langle n_i + n_j \rangle$	$\langle n_i n_j \rangle$
I	0	0	0
II	0.629	0.629	0
III	0.629	1.371	0.371
IV	0	2	1

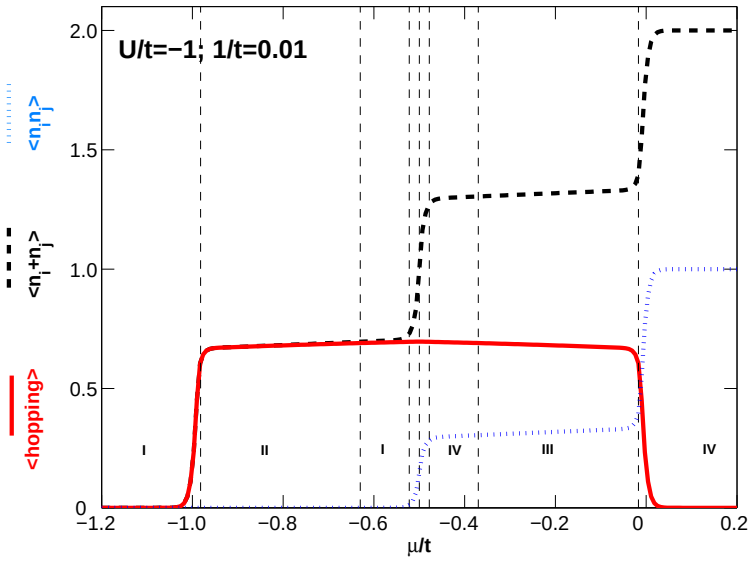

Figure 3.2: Expectation values for $1/t = 0.01$, $U/t = -1$.

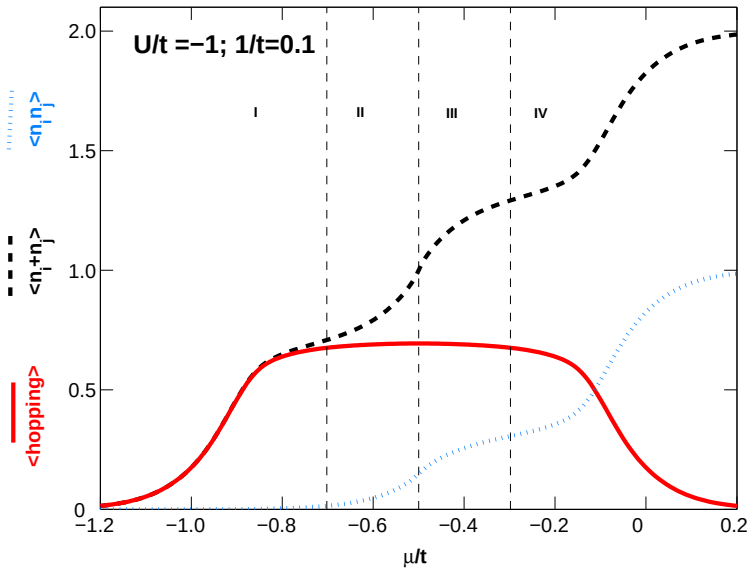

Figure 3.3: Expectation values for $1/t = 0.1$, $U/t = -1$.

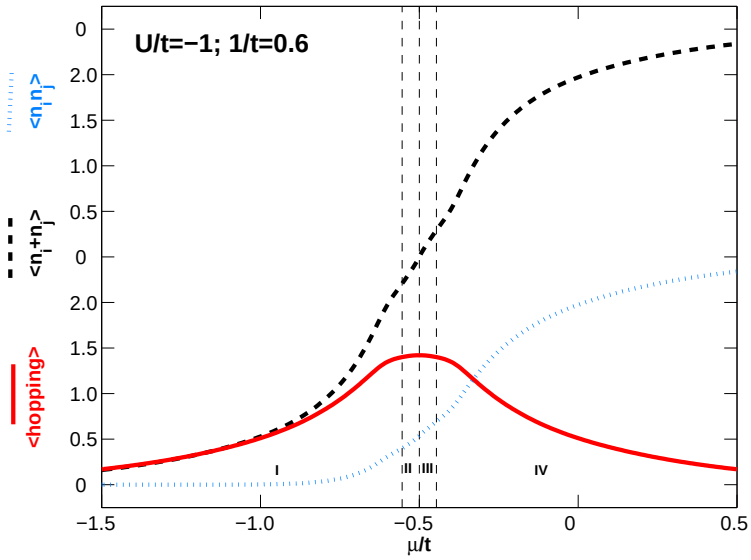

Figure 3.4: Expectation values for $1/t = 0.6$, $U/t = -1$.

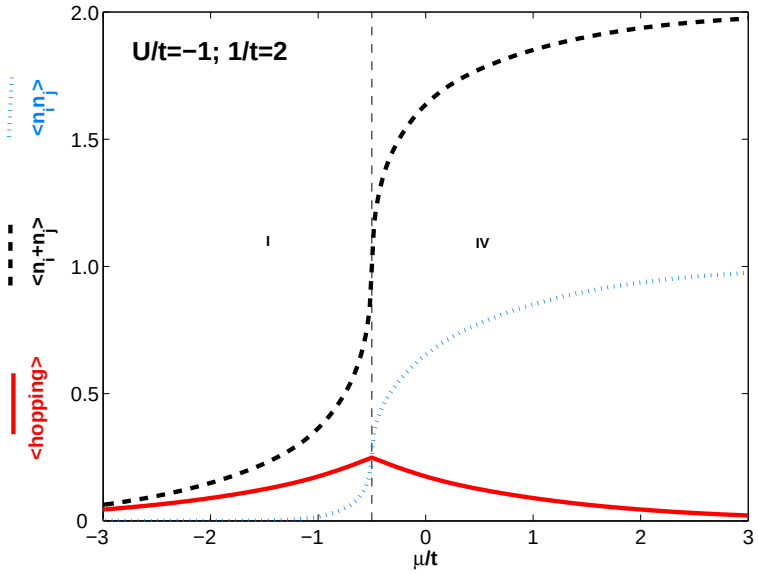

Figure 3.5: Expectation values for $1/t = 2$, $U/t = -1$.

4. CONCLUSION

Throughout this thesis, attention was given to phase transitions taking place in classical and quantum systems, with specific applications of renormalization-group theory to the Blume-Emery-Griffiths and Hubbard models. As far as the classical system is concerned, the detailed phase diagrams of the Blume-Emery-Griffiths spin glass were calculated with the inclusion of quenched randomness to the system. The effects of impurity addition to the ordered system were demonstrated and the appearance of a spin-glass phase and evolution of the first- and second-order phase transitions were witnessed as well as a strong-coupling second-order transition. The topology of the BEG spin-glass was found to have inverted tricritical points, first-order transitions replacing second-order transitions as temperature is lowered. Also, the phase diagrams had disconnected spin-glass regions, spin-glass and paramagnetic reentrances and complete reentrance, where the spin-glass phase completely replaced the ferromagnetic phase as temperature was lowered for all chemical potentials. The phase diagrams were determined by the basins of attraction of the renormalization-group sinks, namely the completely stable fixed points and fixed distributions in the parameter space of the interaction constants J,K,Δ and $\Delta^{\dagger}$. With this analysis, it was found that for Δ/J greater than 0.192 first-order transitions between the ferromagnetic and paramagnetic phases start to appear. When $\Delta/J > 0.34$, second-order transitions completely change to strong coupling transitions, which also disappear for $\Delta/J > 0.42$.

In the quantum system chapter, the spinless hard-core Hubbard model was studied for fermions. The phase diagrams and the expectation values of the interaction terms were calculated and presented in the study. It was found that the system had four different phases, all of which were separated by second-order phase transitions. The phases found were a dilute phase, a dense phase and two intermediate phases where the hopping of fermions takes place. While calculating

the recursion relations of this model, the Suzuki-Takano approximation was used to do the necessary decimation. Although the phase diagrams are not presented, the same analysis was done on a system of bosons where each site can be doubly occupied. In the investigation of this situation (and of the n-particle situation) the inclusion of randomness and long-range interactions are the future prospects that should be considered.

REFERENCES

[1] **Stanley, H.E.**, 1987. Introduction to Phase Transitions and Critical Phenomena, Oxford University Press, New York.

[2] **Yeomans, J.M.**, 1992. Statistical Mechanics of Phase Transitions, Clarendon Press, Oxford.

[3] **Kadanoff, L.P.**, 2000. Statistical Physics: Statics, Dynamics and Renormalization, World Scientific, Singapore.

[4] **Berker, A.N.**, **Ostlund, S. and Putnam, F.A.**, 1978. Renormalization-group treatment of a Potts lattice gas for krypton adsorbed onto graphite, *Phys. Rev. B*, **17**, 3650.

[5] **Chaikin, P.M. and Lubensky, T.C.**, 1995. Principles of Condensed Matter Physics, Cambridge University Press, Cambridge.

[6] **Collins, J.C.**, 1984. Renormalization: An Introduction to Renormalization, the Renormalization Group, and the Operator-Product Expansion, Cambrdige University Press, Cambridge.

[7] **Binder, K. and Young, A.P.**, 1986. Spin glasses: Experimental facts, theoretical concepts, and open questions, *Reviews of Modern Physics*, **58**.

[8] **Berker, A.N. and Ostlund, S.**, 1979. Renormalization-group calculations of finite systems: order parameter and specific heat for epitaxial ordering, *J. Phys. C*, **12**, 4961.

[9] **Griffiths, R.B. and Kaufman, M.**, 1982. Spin systems on hierarchical lattices. Inroduction and thermodynamic limit, *Phys. Rev. B*, **26**, 5022.

[10] **Kaufman, M. and Griffiths, R.B.**, 1984. Spin systems on hierarchical lattices. II. Some examples of soluble models, *Phys. Rev. B*, **30**, 244.

[11] **Blume, M.**, **Emery, V.J. and Griffiths, R.B.**, 1971. Ising model for the λ transition and phase separation in $He^3 - He^4$ mixtures, *Phys. Rev. A*, **4**, 1071.

[12] **Berker, A.N. and Wortis, M.**, 1976. Blume-Emery-Griffiths-Potts model in two dimensions: Phase diagram and critical properties from a position-space renormalization group, *Phys. Rev. B*, **14**, 4946.

[13] **Nishimori, H.**, 2001. Statistical Physics of Spin Glasses and Information Processing, Oxford University Press, New York.

[14] **Falicov, A. and Berker, A.N.**, 1996. Tricritical and critical end-point phenomena under random bonds, *Phys. Rev. Lett.*, **76**, 4380.

[15] **Erbaş, A.**, **Tuncer, A.**, **Yücesoy, B. and Berker, A.N.**, 2005. Phase diagrams and crossover in spatially anisotropic $d = 3$ Ising, XY magnetic and percolation systems, *Phys. Rev. E.*, **72**, 026129.

[16] **Hinczewski, M. and Berker, A.N.**, 2005. Multricritical point relations in three dual pairs of hierarchical-lattice Ising spin glasses, *Phys. Rev. B*, **72**, 144402.

[17] **Migliorini, G. and Berker, A.N.**, 1998. Global random-field spin-glass phase diagrams in two and three dimensions, *Phys. Rev. B.*, **57**, 426.

[18] **Nobre, F.D.**, 2001. Phase diagrams of the two-dimensional $\pm J$ Ising spin-glass, *Phys. Rev. E.*, **64**, 046108.

[19] **Hui, K. and Berker, A.N.**, 1989. Random-field mechanisms in random-bond multicritical systems, *Phys. Rev. Lett.*, **62**, 2507; erratum **63**, 2433 (1989).

[20] **Aizenman, M. and Wehr, J.**, 1989. Rounding of first-order phase transitions with quenched disorder, *Phys. Rev. Lett.*, **62**, 2503; erratum **64**, 1311 (1990).

[21] **Anderson, P.W.**, 1988. *Science*, **235**, 1196.

[22] **Mott, N.F.**, 1968. Metal-insulator transition, *Rev. Mod. Phys.*, **40**, 677.

[23] **Zhang, F.C. and Rice, T.M.**, 1988. Effective hamiltonian for the superconducting Cu oxides, *Phys. Rev. B.*, **37**, 3759.

[24] **Stewart, G.R.**, 1984. Heavy-fermion systems, *Rev. Mod. Phys.*, **56**, 765.

[25] **Fulde, P.**, **Keller, J. and Zwicknagl, G.**, 1988. Theory of heavy fermion systems, *Solid State Phys.*, **41**, 1.

[26] **Bednorz, J.G. and Müller, K.A.**, 1986. Possible high T_c superconductivity in the Ba-La-Cu-O systems, *Z. Phys. B*, **64**, 189.

[27] **Suzuki, M. and Takano, H.**, 1979. Migdal renormalization group approach to quantum spin systems, *Phys. Lett. A*, **69**, 426.

[28] **Takano, H. and Suzuki, M.**, 1981. Migdall-Kadanoff renormalization group approach to the spin-1/2 anisotropic Heisenberg model, *J. Stat. Phys.*, **26**, 635.

BIOGRAPHY

Ongun Özçelik was born in Kocaeli-Turkey, in 1982. He graduated from Robert College in 2000 and in the same year entered the Mechanical Engineering Department of Istanbul Technical University. He graduated from I.T.U with a double major from Mechanical Engineering and Physics in the fall semester of 2005. He started his M.Sc education in spring 2006 in the Physics Department of the same university. Since then, he has been continuing his education in that department under the supervision of Prof. Nihat Berker and with the support of the Science Training Group of TÜBİTAK.